Desalination and Water Treatment
www.deswater.com

doi: 10.5004/dwt.2019.24390

163 (2019) 224–232
September

A novel rose-like polyaniline/Bi_2WO_6 nanocomposite: synthesis and its application in photocatalysis

Limin Zhao, Xin Shao, Min Wang, Hui Zhao, Bo Ge, Wenzhi Li*

College of Materials Science and Engineering, Liaocheng University, Liaocheng 252059, China, emails: liwenzhi@lcu.edu.cn (W. Li), zhaolimin@lcu.edu.cn (L. Zhao), shaoxin@lcu.edu.cn (X. Shao), wangmin@lcu.edu.cn (M. Wang), zhaohui@lcu.edu.cn (H. Zhao), gebo@lcu.edu.cn (B. Ge)

Received 9 January 2019; Accepted 13 May 2019

ABSTRACT

A novel three-dimensional (3D) rose-like Bi_2WO_6 hierarchical architecture with high surface area is successfully prepared by a chemical method and then coated with polyaniline (PANi) through a simple method. The prepared samples are characterized using X-ray diffraction, X-ray photoelectron spectroscopy and scanning electron microscopy. The photocatalytic activities of PANi/Bi_2WO_6 composite are evaluated through the degradation of rhodamine B (RhB). The excellent performance of the PANi/Bi_2WO_6 composite could be owing to the unique rose-like structure and rapid separation efficiency of the photogenerated electron–hole pairs between PANi and Bi_2WO_6. The stability of the composite is found to be satisfying, which makes it potential in practical application.

Keywords: Hierarchical architecture; Dye degradation; Photocatalytic activity

1. Introduction

The harmful organic pollutants in water have caused environmental problems and become a great challenge for sustainable development. During the past decades, the researchers pay attention into semiconductor photocatalysts because of their wide applications in degradation of organic contaminants and solar energy conversion under ultraviolet or visible-light [1–5]. To efficiently utilize sunlight, researchers have studied a wide range of visible light-induced photocatalysts. Some novel visible light-induced photocatalyst, such as WO_3, ZnO, Ag_3PO_4, CdS, Bi-based ternary oxides, etc., has been reported [6–12]. Among them, Bi_2WO_6 is special and paid more attention for its good chemical and physical performance [13–17]. Zhang and Zhu [18] have reported that Bi_2WO_6 can effectively liberate oxygen from water and degrade of organic pollutants in water expose in the visible light.

As is well known, the morphology, size and structure of the photocatalysts can significantly affect its photocatalytic activities [19]. As a new nanostructure, hierarchical structures attributed to their nano/micro combined architectures have aroused much research interest [20–22]. To improve photocatalytic property, many recent efforts have been made to achieve controllable synthesis of highly ordered Bi_2WO_6 hierarchical structures with specific shape. In previous reports, nest-like [23,24], microspheric [25], nanocages-like [26], tyre-/helix-like [27] and clew-like [28] Bi_2WO_6 hierarchical architectures have been synthesized. Compared with other hierarchical architectures, flower-like or rose-like Bi_2WO_6 has a rather large surface area and attracts increasing attention [29]. He et al. [30] successfully synthesized hierarchical rose-like Bi_2WO_6 photocatalyst through a simple hydrothermal route with acetic acid and thiourea as complexing agents. But these hierarchical architectures were constructed from plenty of flat nanoplates

* Corresponding author.

which are unfavorable to the increasing specific surface area. Therefore, the ability for degrading organic dyes is confined and ought to be enhanced. In addition, the preparation of Bi_2WO_6 through hydrothermal process required a higher temperature. Then, the formation of uniform and high surface area Bi_2WO_6 nano-power still is a challenge. In order to further improve the photocatalytic activity of Bi_2WO_6, increasing separation efficiency of photogenerated electron–hole pairs is another effective way [31]. The polyaniline (PANi) has an excellent electronic conductivity due to its important intrinsically conducting polymers. Taking account of its carrier transfer efficiency, PANi has showed great promises in enhancing separation efficiency of photogenerated electron–hole pairs. Through a facile chemical method, Laabd et al. [32] had synthesized PANi/Bi_2WO_6 nanocomposites. Wang et al. [33] had prepared Bi_2WO_6 photocatalyst modified by PANi through in situ polymerization of vapor phase aniline. However, the Bi_2WO_6 particle in these composites was consisting of spheres or fiber-like morphologies.

In this study, a novel 3D rose-like Bi_2WO_6 hierarchical architecture with high surface area was prepared through a simple reflux method in aqueous solution using dodecylamine as a morphology adjustor. Then PANi was coated into the 3D Bi_2WO_6 hierarchical architecture with chemical method and PANi/Bi_2WO_6 composite was synthesized. The prepared Bi_2WO_6 hierarchical architecture was formed by thin curved petaloid flake and the novel structure can be favorable to the transfer and separation of electron–hole pairs. Structural, morphological and the removal efficiency of Rhodamine B (RhB) pollutant in aqueous medium of the prepared composites were discussed and investigated.

2. Experiment

2.1. Preparation of rose-like Bi_2WO_6

In a typical procedure, 1.4550 g $Bi(NO_3)_3{\cdot}5H_2O$ (3.0 mmol) was dissolved in 50 mL of 0.5 M nitric acid solution in a beaker (A). 0.4948 g $Na_2WO_4{\cdot}2H_2O$ (1.5 mmol) was dissolved in 50 mL water (B). Then, the solution B was dropwise added to the solution A with stirring intensely. These solutions were agitated for about 30 min resulting in a homogeneous solution. After that, 6 mL dodecylamine was added into the solution and stirred for 30 min to get the precursor. Afterwards, the precursor was transferred to the three-necked round bottom flask with condenser tube. The reaction solution was stirred in an oil bath for 24 h at 120°C. The final product was centrifuged and washed three times with deionized water and absolute ethanol. Therefore, the sample was dried at 80°C for 20 h and named as B0.

2.2. Synthesis of the PANi/Bi_2WO_6 composite

The PANi/Bi_2WO_6 composite was synthesized by chemical oxidative polymerization of aniline monomer in the presence of rose-like Bi_2WO_6 in acidic solution. A typical synthesis procedure can be described briefly as follows: 0.50 g rose-like Bi_2WO_6 was dispersed in 50 mL of HCl (1 M) by ultrasonic vibration for 30 min. Then, the aniline monomer (10, 20 and 30 μL, respectively) was added into the mixture and treated by ultrasonic vibration for 30 min. After that, 50 mL of sodium persulfate solution (molar ratio of aniline/oxidant = 1/1) was slowly added dropwise to the mixture. The polymerization reaction continues under magnetic stirring for 12 h at room temperature. Finally the PANi/Bi_2WO_6 composite with different contents of PANi was centrifuged and washed three times with deionized water and absolute ethanol to remove the soluble impurities, and then dried at 70°C for 12 h. The samples with different contents of PANi were named as BP1, BP2 and BP3, respectively.

2.3. Characterizations

X-ray diffraction (XRD) patterns are collected on a Bruker AXS D8 powder diffractometer at scanning rate of 0.025 S^{-1} (Bruker, German). The chemical states of samples are characterized by X-ray photoelectron spectroscopy (XPS) in a Thermo Fisher Scientific Escalab 250 spectrometer with monochromatized Al Kα excitation, and C_{1s} (284.6 eV) is used to calibrate the peak positions of the elements. The field-emission scanning electron microscopy (FESEM, Zeiss Merlin Compact, German) and high-resolution TEM (HR-TEM, FEI Tecnai G2 F20, USA) are used for characterizing the morphologies of the samples. UV-Vis diffuse reflectance spectra are recorded on a PerkinElmer Lambda 900 spectrophotometer equipped with an integrating sphere. The Brunauer–Emmett–Teller (BET) surface areas, pore size distribution, nitrogen adsorption and desorption isotherm are determined at 77 K with a Quantachrome NOVA 4000e Analyzer.

2.4. Photocatalytic experiment

Photocatalytic performances of rose-like Bi_2WO_6 and composites are measured in a homemade reaction box. A 300-W Xe lamp (Beijing Perfectlight Co. Ltd, China, 320 nm ≤ λ ≤ 780 nm) is employed as simulated solar light and placed about 10 cm on a cylindrical jacket beaker with a cooling water. 0.05 g Bi_2WO_6 is added into 100 mL 10 mg L^{-1} RhB solution and treated for 5 min in an ultrasonic bath. In order to establish an adsorption–desorption equilibrium between the samples and RhB solution, the suspensions are stirred in the dark for 55 min. At 20 min interval, 5 mL of sample solution is extracted during the photocatalysis. Then the absorption of solution is measured on a UV–vis spectrophotometer after 3 min of centrifugation. Four-cycle photodegradation for RhB is used out for characterizing the stability of as-obtained PANi/Bi_2WO_6 composite and each cycle lasts for 120 min. The samples are washed with water and absolute alcohol three times after each cycle, and re-dispersed in new RhB solution for the next photodegradation.

3. Results and discussion

3.1. Structure and morphology

Fig. 1 shows the XRD pattern of rose-like Bi_2WO_6 and composites. All diffraction peaks of pure Bi_2WO_6 can be indexed as orthorhombic phase of Bi_2WO_6 (JCPDS card No. 73-1126) and without any impurities or other phases are detected. The diffraction peaks are broader which means

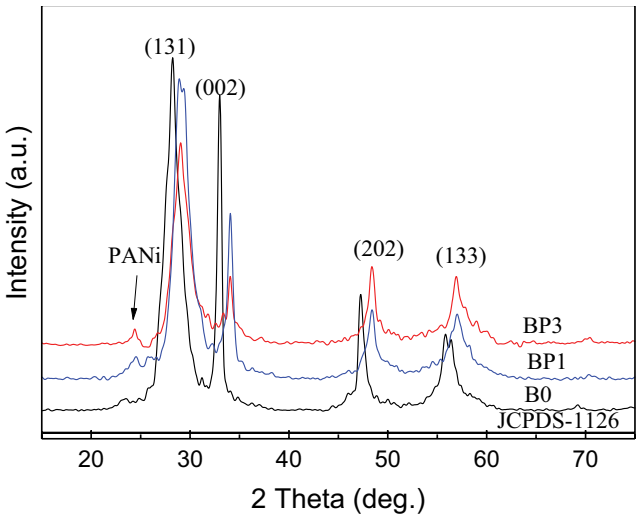

Fig. 1. XRD pattern of pure Bi_2WO_6 and PANi/Bi_2WO_6 composite.

the crystalline grain of samples is small. Compared with pure Bi_2WO_6, the diffraction peaks of PANi/Bi_2WO_6 composite show an obvious shift to higher degrees (Fig. 1), which may be ascribed to the presence of a structural disorder in the Bi_2WO_6 matrix. Further analysis of the patterns shows no additional peaks associated to PANi implying that the amount used to modify the bismuth tungstate is small.

Fig. 2 shows the XPS spectra of the pure Bi_2WO_6 and PANi/Bi_2WO_6 composite. The binding energy peaks of B0 in Fig. 2a are assigned to Bi 4f, Bi 4d, Bi 4p, W 4f, W 4d, O 1s and O auger state, respectively. These indicate that all the samples consist of Bi, W and O elements, which is consistent with the result of EDS (Fig. 4). Compared with pure Bi_2WO_6, there is a weak peak located at about 399 eV in the spectra of PANi/Bi_2WO_6 composite. This peak belongs to the N 1s, which means the PANi has been compounded with the Bi_2WO_6. The XPS spectra in Fig. 2c belong to the W^{6+} $4f_{7/2}$ and $4f_{5/2}$ states at 35.5 and 37.6 eV, respectively [34] and the XPS spectra in Fig. 2d belong to the Bi^{3+} $4f_{7/2}$ (159.4 eV) and $4f_{5/2}$ (164.8 eV) states [35]. In addition, the binding energy peak in Fig. 2b at 530.5 eV is assigned to O 1s state in Bi_2WO_6.

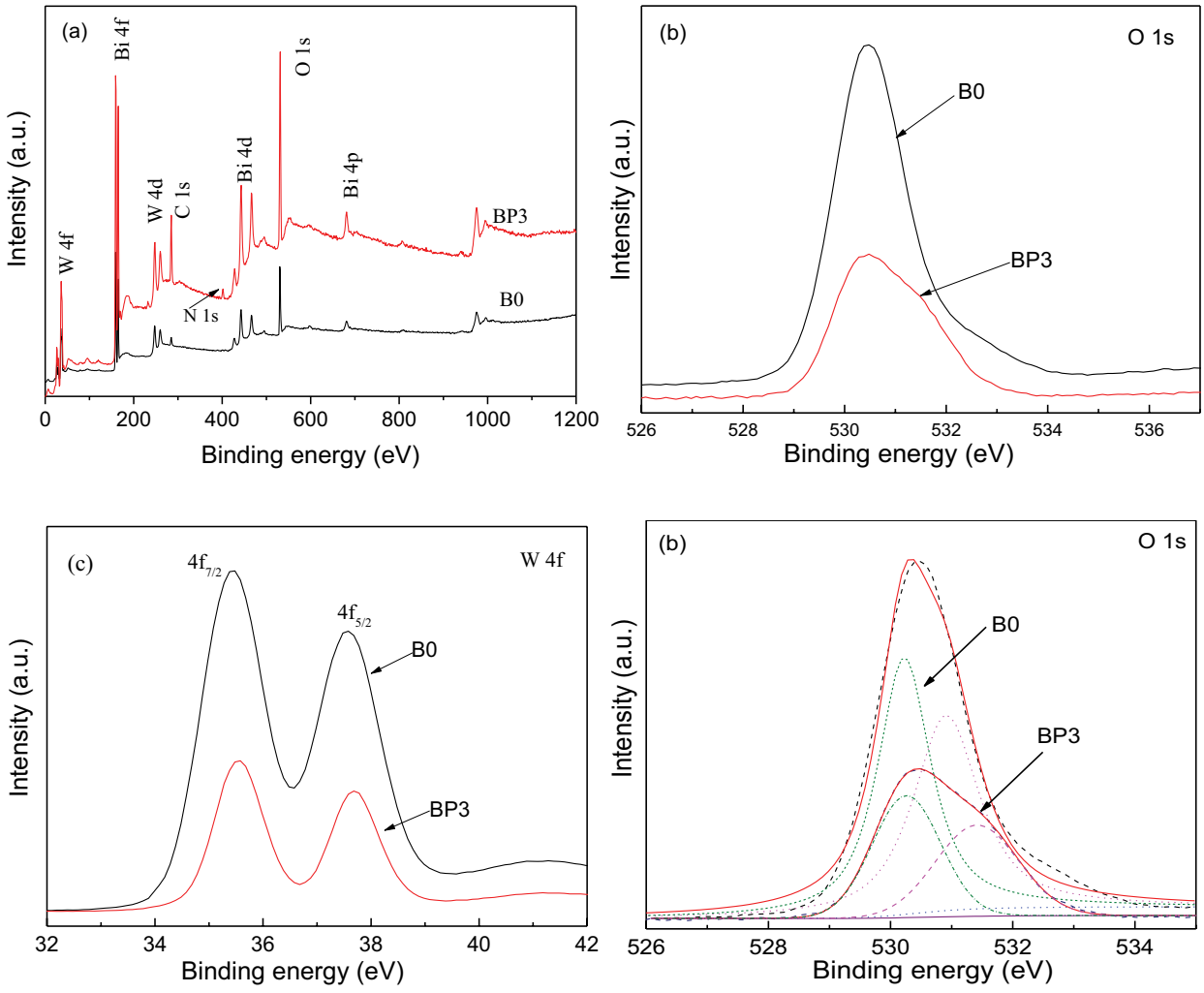

Fig. 2. XPS data of pure Bi_2WO_6 and PANi/Bi_2WO_6 composite: (a) the whole-range spectrum, (b) O 1s core-level spectrum, (c) W 4f core-level spectrum, and (d) Bi 4f core-level spectrum.

The O 1s XPS signal can be deconvoluted into two peaks at 529.8 and 531.5 eV. The binding energy at 529.8 eV belongs to the crystal lattice oxygen of Bi_2WO_6. The peaks at higher binding energies of 531.5 could arise from surface defects or chemisorbed oxygen species [36].

The morphology of Bi_2WO_6 samples is confirmed by FESEM. At a low magnification view in Fig. 3a, the morphology of B0 shows large-scale monodispersed rose-like hierarchical structure with diameter of 2–4 m. These rose-like hierarchical structures are constructed by thin petaloid Bi_2WO_6 flake. The high-magnification SEM image is shown in Fig. 3b. From this picture, we can observe that several thin petaloid Bi_2WO_6 flake of about 20 nm in thickness are joined to form a rose-like hierarchical structure. For further demonstrating the composition of hierarchical structure, EDS is performed. Fig. 4a shows the EDS spectra of rose-like Bi_2WO_6 which demonstrates that the samples consist of Bi, W and O. The atomic ratio of Bi:W:O is approximately to 2:1:6. From the EDS mapping (Figs. 4b–e), it can be found that the elements Bi, O and W are evenly distributed in the as-prepared samples. Fig. 5 shows the HRTEM images of an individual thin petaloid Bi_2WO_6 flake of B0 samples. The clear lattice fringes can be observed in the edge of thin petaloid Bi_2WO_6 flake. The interplanar spacing of B0 is 0.272 nm, which is corresponding to the (200) plane of orthorhombic Bi_2WO_6. At the bottom and top surfaces of petaloid Bi_2WO_6 flake, the interplanar spacing of B0 sample is 0.324 nm and according with to the (113) plane of orthorhombic Bi_2WO_6. The percentage of (113) facets is estimated from the geometric calculation to be ca. 95% for the B0 sample. Fig. 6 shows the SEM and HRTEM images of PANi/Bi_2WO_6 composite (BP3). It can be seen that the size and morphology of BP3 are almost unchanged. The composite has a smooth surface. All these show that PANi can well disperse on the surface of Bi_2WO_6. Furthermore, the HRTEM image (left) of BP3 displays a distinct PANi noncrystal edge, indicating a close contact between Bi_2WO_6 and PANi.

3.2. Photodegradation

The particle size and surface area of samples are closely related to its photocatalytic behavior. BET gas-sorption measurements are used to investigate the porous structure of prepared rose-like Bi_2WO_6. As shown in Fig. 7, pure Bi_2WO_6 and PANi/Bi_2WO_6 composite all display a typical character of type-IV isothermal in the IUPAC classification, which are characteristic of porous materials. Meanwhile, the corresponding pore diameter distributions of all samples (the insert of Fig. 7) are centered at about 3.7 nm. The BET surface areas of all samples are shown in Table 1 and the surface area of B0 samples without PANi is 42.6 m^2/g. The surface areas of PANi/Bi_2WO_6 composite with different amount PANi are 33.4, 38.4, 42.3 and 35.6 m^2/g, respectively. The change in surface area may be due to the introduction of polyaniline. Contrast to the Bi_2WO_6 matrix, the surface areas of BP3 changed little, which means it may have higher photocatalytic activity.

As well known, the energy band structure of a semiconductor is closely related to its photocatalytic activity [37]. Fig. 8 shows the UV–Vis absorption spectra (DRS) of all samples. In the visible region, all samples have the strongly absorption bands with steep edges. According to the literature, the steep shape of the spectra indicates that the visible-light absorption is due to the band-gap transition rather than the transition from the impurity [38]. Contrast with the pure Bi_2WO_6, the DRS spectra of PANi/Bi_2WO_6 composite changed a little. Bi_2WO_6 is a direct band gap semiconductor. Estimating through the plots of $(\alpha h\nu)^2$ versus $h\nu$ (inset of Fig. 8), the band gap of BP3 and B0 samples are about 2.77 and 2.67 eV, respectively [39]. It means B0 sample can absorb more visible light than BP3 and electrons in B0 sample are more easily excited from the VB to CB.

The photocatalytic activity of as-prepared Bi_2WO_6 and PANi/Bi_2WO_6 composite is assessed through degrading rhodamine B (RhB) solution under simulated solar irradiation. A xenon lamp is used to simulate the solar irradiation. Fig. 9a shows the absorption spectra of RhB solution after degradation by the prepared PANi/Bi_2WO_6 composite BP3. It can be seen that the absorption of RhB at 554 nm decreased which demonstrate the decomposition of RhB. As the irradiation time prolonged, the maximum absorption wavelength of RhB solution is observed decreased and shows blue-shift from 554 to 495 nm. Correspondingly, the color of solution changes from pink to light green. Based on previous reports, the blue-shift of absorption peak is usually attributed to the de-ethylated degradation process and formation of a series of N-deethylated intermediates and in a stepwise manner [40]. The dynamic curves of photodegradation are shown in

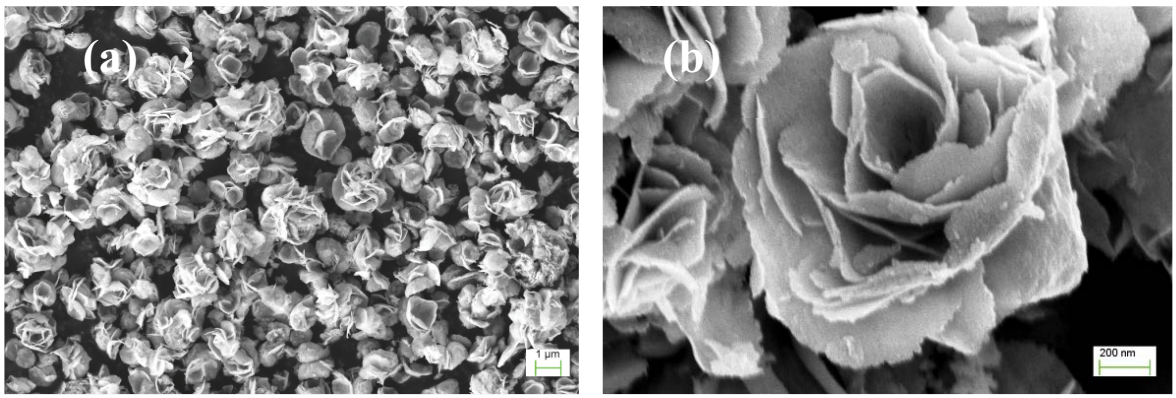

Fig. 3. FESEM images Bi_2WO_6 (B0): (a) panoramic FESEM image and (b) amplified FESEM image.

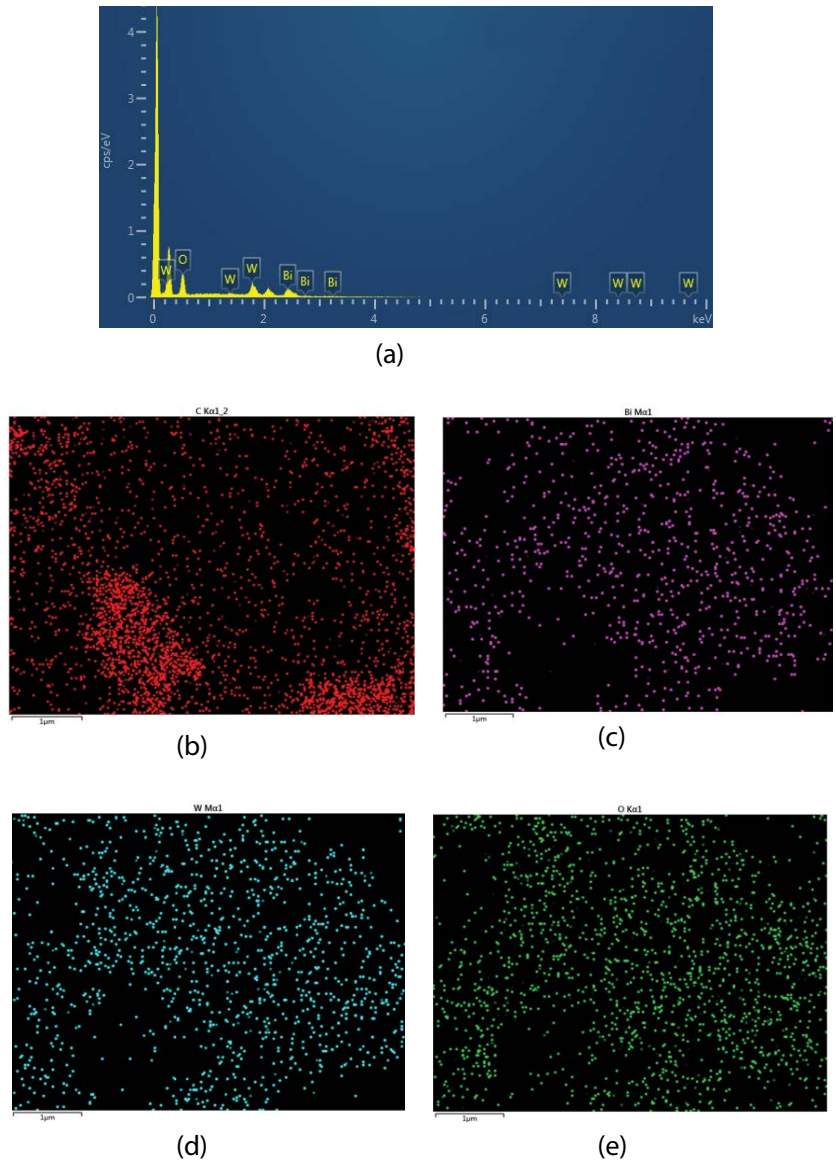

Fig. 4. Energy dispersive spectroscopy spectrum (a) of pure Bi_2WO_6 (B0) and mapping image (b–e).

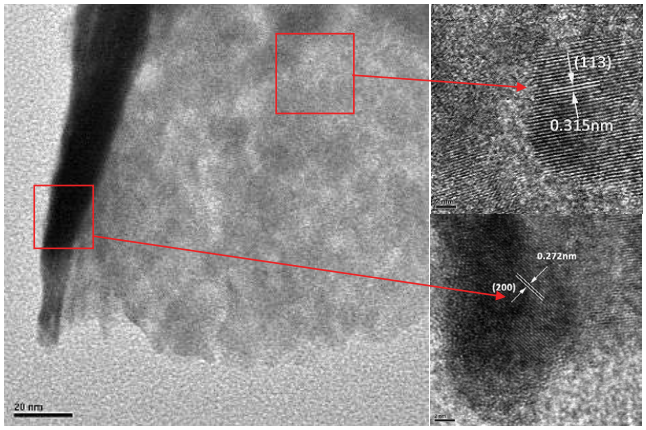

Fig. 5. HR-TEM images of the individual petaloid nanoflake units (B0).

Fig. 9b. It is found that the degradation of RhB hardly occurs with the absence of photocatalyst. Furthermore, RhB is completely degraded in 20 min with the BP3 sample, which is obviously higher than B0 and other PANi/Bi_2WO_6 composite. This means BP3 sample has the best photocatalytic efficiency. Fig. 9c shows the plots of $\ln(C_0/C)$ vs. the illumination time. As can be seen, the process of photodegradation RhB conforms to the pseudo-first-order kinetics equation [41]. The removal rate constant k of photocatalytic degradating RhB with BP3 is 0.107 min^{-1}, which is about 2.4 and 180 times that of B0 (0.044 min^{-1}) and blank (5.93×10^{-4} min^{-1}), respectively. For evaluating the stability and reusability of the as-prepared PANi/Bi_2WO_6 composite, four recycling experiments of BP3 sample for the photodegradation of RhB are performed (Fig. 9d). After being used four times for RhB degradation, the photocatalytic performence of BP3 is not obvious decreased. This result indicates that the as-prepared

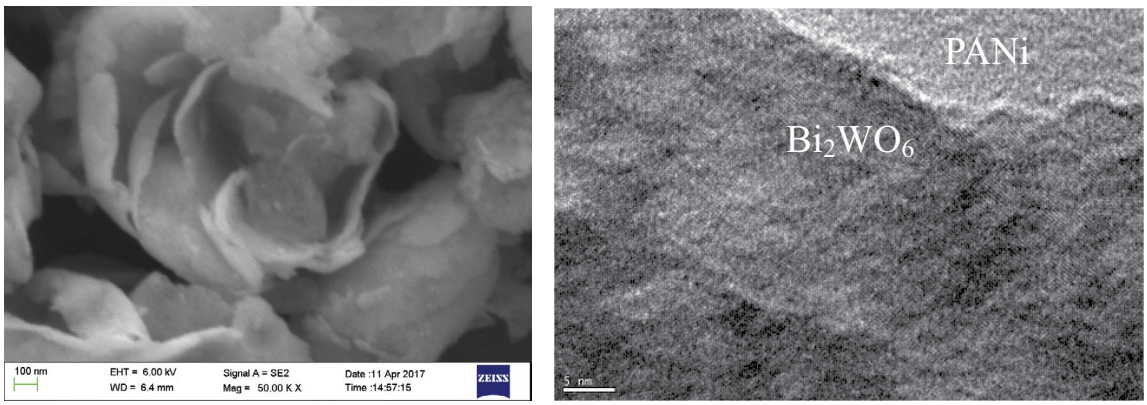

Fig. 6. FE-SEM images and HR-TEM images of BP3.

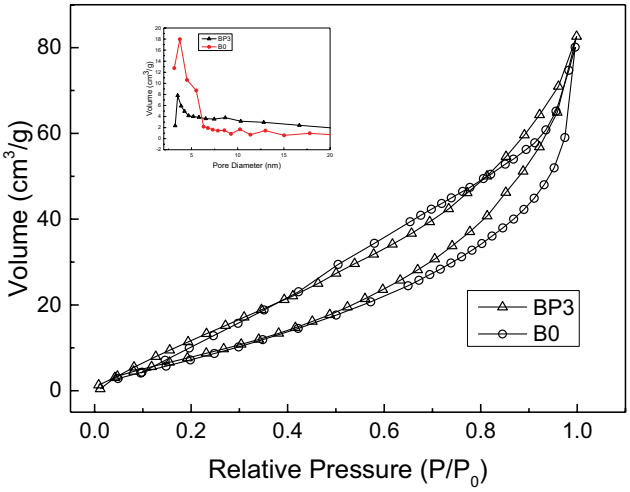

Fig. 7. N_2 adsorption–desorption curves and pore diameter distributions (inset) of B0 and BP3.

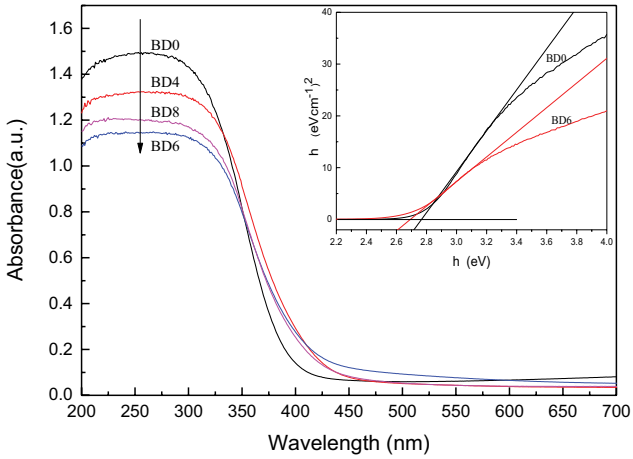

Fig. 8. UV–vis DRS and plots of $(\alpha h\nu)^{1/2}$ vs. hν (the inset) of samples.

Table 1
BET surface of the samples

Sample	S_{BET} (m^2/g)
B0	42.6
BP1	33.4
BP2	38.4
BP3	42.3

$PANi/Bi_2WO_6$ composite shows high photocatalytic activity and stability. From the result of DRS spectra, B0 sample can absorb more visible light than BP3. Nevertheless, its photocatalytic efficiency is less than BP3 sample. This means the improvement of photocatalytic performance in $PANi/Bi_2WO_6$ composite is mainly according to the rapid separation efficiency of the photogenerated electron–hole pairs between PANi and Bi_2WO_6. The formation of $PANi/Bi_2WO_6$ composite makes the separation of photogenerated electron–hole pairs more easily.

For studying the degradation mechanism of $PANi/Bi_2WO_6$ composite, some scavengers are used to explore the type of reactive species in the RhB degradation process. The results are shown in Fig. 10. The photocatalytic performance of BP3 does not change with the addition of isopropanol as scavenger for •OH [42], which indicates that it is not the major oxidative species in the RhB photodegradation with BP3 samples. When the EDTA-2Na (a kind of h^+ scavenger) is added into the reaction system, the photocatalytic reaction is obviously inhibited. With the addition of KI, a scavenger for hole and •OH [43], the degradation rate of RhB was obviously decreased than that of no scavengers. These results indicate that hole may be a predominant active species responsible for the photocatalytic reaction.

It is well known that the photocatalytic activity of semiconductor is closely related to the band edge position, an intrinsic property of semiconductor. Then we calculate the conduction band (CB) and valence band (VB) edge position of semiconductor at the point of zero charge through the empirical equation [44]: $E_{CB} = \chi - E_e - 0.5E_g$. Where χ is the absolute electronegativity of semiconductor, and E_e is the free electrons energy on the hydrogen scale (4.5 eV). For Bi_2WO_6, χ is 6.360 eV and E_g is 2.67 eV. Then the CB bottom (E_{CB}) of Bi_2WO_6 is 0.525 eV calculated through the equation above. Simultaneously, the VB top (E_{VB}) is 3.195 eV. Fig. 11 illustrates the electron–hole pairs generated over

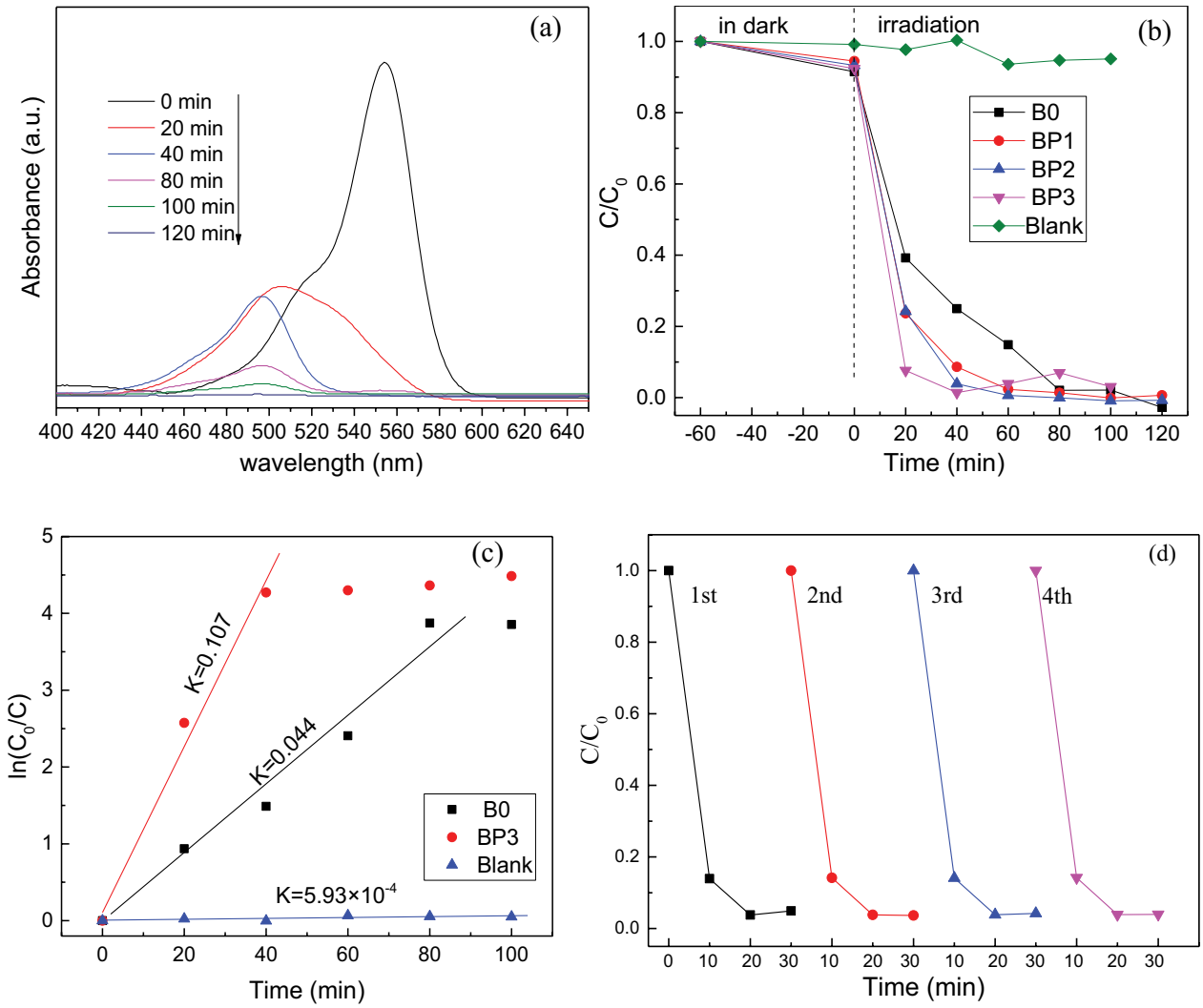

Fig. 9. Absorption evolution of RhB solution for BP3 in photocatalytic process (a), dynamic curves of photodegradation (b), plots of $\ln(C_0/C)$ vs. time for RhB solutions over different samples (c), cycling photodegradation runs (d) for RhB solutions over BP3 samples.

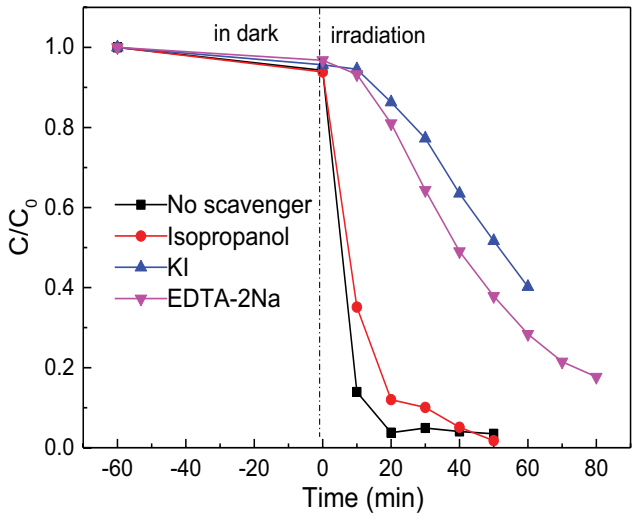

Fig. 10. Dynamic curves of photodegradation with scavengers over BP3 sample.

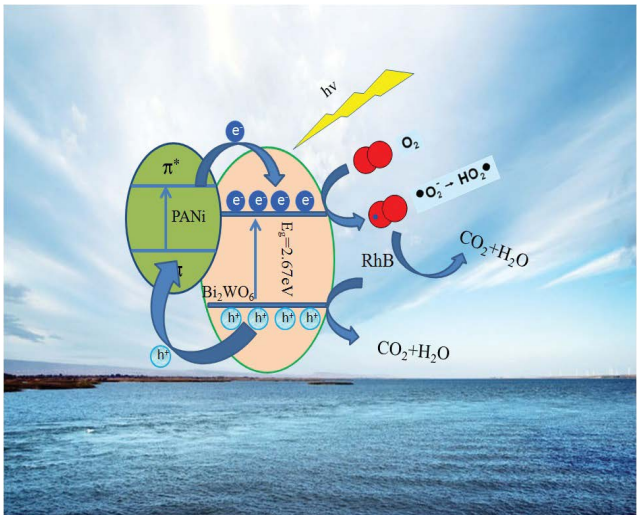

Fig. 11. Schematic diagram illustrating the photocatalytic redox reactions.

PANi/Bi_2WO_6 composite under irradiation. Under simulated sunlight irradiation, electrons are excited from the valence band (VB) of Bi_2WO_6 to its CB, thus creating electron/hole pairs. Simultaneously, the electronic excitation process also occurs in PANi. The photoexcited PANi are excellent electron donors and electron acceptors [45]. As a result, the holes generated from valence band of Bi_2WO_6 can be directly transfered to the π orbital of PANi. Meanwhile, the photogenerated electrons can be transfered from PANi to the conduction band of Bi_2WO_6. This leads to the separation and stabilization of photogenerated charge, thus preventing the recombination of photogenerated electron–hole pairs. Simultaneously, the photogenerated electrons on the conduction band of Bi_2WO_6 can be captured by O_2 to yield $^{\bullet}O_2^-$ and $^{\bullet}OOH$. The photogenerated holes and these radicals can easily transfer to the surface of PANi/Bi_2WO_6 composite and react with the adsorbing RhB. Furthermore, the RhB molecules are oxidized with forming CO_2 and H_2O.

4. Conclusions

In conclusion, a novel rose-like Bi_2WO_6 hierarchical nanostructures constructed by thin petaloid flake was successfully synthesized through a simple reflux method. Then we successfully prepared and characterized PANi/Bi_2WO_6 composites. The obtained experimental data showed that the pure rose-like Bi_2WO_6 had a wider range of light absorption, but the PANi/ Bi_2WO_6 composites had a higher removal efficiency of RhB dye. The excellent properties of the PANi/ Bi_2WO_6 composite were mainly ascribed to the rapid separation and slow recombination of the photogenerated electron–hole pairs.

Acknowledgments

This work was supported the financial support of the National Natural Science Foundation of China (Grant No. 51072075), the Foundation of Shandong training project (Grant No. ZR2018PB014 and ZR2019PB017), and Research start fund of Liaocheng University (318051508 and 318011404).

References

[1] A. Fujishima, K. Honda, Electrochemical photolysis of water at a semiconductor electrode, Nature, 238 (1972) 37–38.
[2] J.H. Carey, J. Lawrence, H.M. Tosine, Photodechlorination of PCB's in the presence of titanium dioxide in aqueous suspensions, Bull. Environ. Contam. Toxicol., 16 (1976) 697–701.
[3] D.D. Zeng, L.M. Yang, P.P. Zhou, D.S. Hu, Y. Xie, S.Q. Li, L.S. Jiang, Y. Ling, J.S. Zhao, Au–Cu alloys deposited on titanium dioxide nanosheets for efficient photocatalytic hydrogen evolution, Int. J. Hydrogen Energy, 43 (2018) 15155–15163.
[4] Z.W. Shao, Y.N. He, T.T. Zeng, Y.N. Yang, X.P. Pu, B. Ge, J.M. Dou, Highly efficient photocatalytic H_2 evolution using the Ni2P-$Zn_{0.5}Cd_{0.5}S$ photocatalyst under visible light irradiation, J. Alloys Compd., 769 (2018) 889–897.
[5] T.T. Zhang, X. Shao, D.F. Zhang, X.P. Pu, Y.X. Tang, J. Yin, B. Ge, W.Z. Li, Synthesis of direct Z-scheme g-C_3N_4/$Ag_2VO_2PO_4$ photocatalysts with enhanced visible light photocatalytic activity, Sep. Purif. Technol., 195 (2018) 332–338.
[6] D. Chen, J. Ye, Hierarchical WO_3 hollow shells: dendrite, sphere, dumbbell, and their photocatalytic properties, Adv. Funct. Mater., 18 (2008) 1922–1928.
[7] B. Weng, M.-Q. Yang, N. Zhang, Y.-J. Xu, Toward the enhanced photoactivity and photostability of ZnO nanospheres via intimate surface coating with reduced graphene oxide, J. Mater. Chem. A, 2 (2014) 9380–9389.
[8] L. Liu, J. Liu, D.D. Sun, Graphene oxide enwrapped Ag_3PO_4 composite: towards a highly efficient and stable visible-light-induced photocatalyst for water purification, Catal. Sci. Technol., 2 (2012) 2525–2532.
[9] T.K. Jana, A. Pal, K. Chatterjee, Self assembled flower like CdS–ZnO nanocomposite and its photo catalytic activity, J. Alloys Compd., 583 (2014) 510–515.
[10] S.H. Liang, T.T. Zhang, D.F. Zhang, X.P. Pu, X. Shao, W.Z. Li, J.M. Dou, One-pot combustion synthesis and efficient broad spectrum photoactivity of Bi/BiOBr:Yb,Er/C photocatalyst, J. Am. Ceram. Soc., 101 (2018) 3424–3436.
[11] Y. Yang, Y. Liu, B. Huang, R. Zhang, Y. Dai, X. Qin, X. Zhang, Enhanced visible photocatalytic activity of a $BiVO_4$@β-$AgVO_3$ composite synthesized by an *in situ* growth method, RSC Adv., 4 (2014) 20058–20061.
[12] M.C. Gao, D.F. Zhang, X.P. Pu, H.Y. Ma, C.H. Su, X. Gao, J.M. Dou, Surface decoration of BiOBr with $BiPO_4$ nanoparticles to build heterostructure photocatalysts with enhanced visible-light photocatalytic activity, Sep. Purif. Technol., 170 (2016) 183–189.
[13] L. Zhang, H. Wang, Z. Chen, P.K. Wong, J. Liu, Bi_2WO_6 micro/nano-structures: synthesis, modifications and visible-light-driven photocatalytic applications, Appl. Catal., B, 106 (2011) 1–13.
[14] C. Li, G. Chen, J. Sun, H. Dong, Y. Wang, C. Lv, Construction of Bi_2WO_6 homojunction via QDs self-decoration and its improved separation efficiency of charge carriers and photocatalytic ability, Appl. Catal., B, 160 (2014) 383–389.
[15] Y. Lv, W. Yao, R. Zong, Y. Zhu, Fabrication of wide–range–visible photocatalyst Bi_2WO_{6-x} nanoplates via surface oxygen vacancies, Sci. Rep., 6 (2016) 19347.
[16] R.F. Tang, H.F. Su, Y.W. Sun, X.X. Zhang, L. Li, C.H. Liu, S.Y. Zeng, D.Z. Sun, Enhanced photocatalytic performance in Bi_2WO_6/SnS heterostructures: facile synthesis, influencing factors and mechanism of the photocatalytic process, J. Colloid Interface Sci., 466 (2016) 388–399.
[17] S. Wang, H. Yang, X. Wang, W. Feng, Surface disorder engineering of flake-like Bi_2WO_6 crystals for enhanced photocatalytic activity, J. Electron. Mater., 48 (2019) 2067–2076.
[18] L. Zhang, Y. Zhu, A review of controllable synthesis and enhancement of performances of bismuth tungstate visible-light-driven photocatalysts, Catal. Sci. Technol., 2 (2012) 694–706.
[19] L.M. Zhao, C.H. Shu, Z.F. Jia, C.Z. Wang, Surface defects control for ZnO nanorods synthesized through a gas-assisted hydrothermal process, J. Electron. Mater., 46 (2017) 432–438.
[20] D. Kuang, T. Brezesinski, B. Smarsly, Hierarchical porous silica materials with a trimodal pore system using surfactant templates, J. Am. Chem. Soc., 126 (2004) 10534–10535.
[21] J.X. Liu, D.F. Zhang, X.P. Pu, J.X. Liu, R.G. Zhang, Combustion synthesis of $Zn_{1-x}Cd_xS$ and its photodegradation performance of methylene blue, Mater. Lett., 117 (2014) 158–161.
[22] C.Y. Sun, Q.H. Xu, Y. Xie, Y. Ling, J.L. Jiao, H.H. Zhu, J.S. Zhao, X.M. Liu, B. Hu, D. Zhou, High-efficient one-pot synthesis of carbon quantum dots decorating Bi_2MoO_6 nanosheets heterostructure with enhanced visible-light photocatalytic properties, J. Alloys Compd., 723 (2017) 333–344.
[23] J. Wu, F. Duan, Y. Zheng, Y. Xie, Synthesis of Bi_2WO_6 nanoplate-built hierarchical nest-like structures with visible-light-induced photocatalytic activity, J. Phys. Chem. C, 111 (2007) 12866–12871.
[24] Y. Tian, G. Hua, W. Xu, N. Li, M. Fang, L. Zhang, Bismuth tungstate nano/microstructures: controllable morphologies, growth mechanism and photocatalytic properties, J. Alloys Compd., 509 (2011) 724–730.
[25] Y. Li, J. Liu, X. Huang, G. Li, Hydrothermal synthesis of Bi_2WO_6 uniform hierarchical microspheres, Cryst. Growth Des., 7 (2007) 1350–1355.
[26] M. Shang, W. Wang, H. Xu, New Bi_2WO_6 nanocages with high visible-light-driven photocatalytic activities prepared in refluxing EG, Cryst. Growth Des., 9 (2008) 991–996.

[27] L. Zhang, W. Wang, L. Zhou, H. Xu, Bi_2WO_6 nano-and microstructures: shape control and associated visible-light-driven photocatalytic activities, Small, 3 (2007) 1618–1625.
[28] D. He, L. Wang, H. Li, T. Yan, D. Wang, T. Xie, Self-assembled 3D hierarchical clew-like Bi_2WO_6 microspheres: synthesis, photo-induced charges transfer properties, and photocatalytic activities, CrystEngComm, 13 (2011) 4053–4059.
[29] C. Zheng, H. Yang, Assembly of Ag_3PO_4 nanoparticles on rose flower-like Bi_2WO_6 hierarchical architectures for achieving high photocatalytic performance, J. Mater. Sci. - Mater. Electron., 29 (2018) 9291–9300.
[30] J. He, W. Wang, F. Long, Z. Zou, Z. Fu, Z. Xu, Hydrothermal synthesis of hierarchical rose-like Bi_2WO_6 microspheres with high photocatalytic activities under visible-light irradiation, Mater. Sci. Eng., B, 177 (2012) 967–974.
[31] X. Wang, J.C. Yu, C. Ho, Y. Hou, X. Fu, Photocatalytic activity of a hierarchically macro/mesoporous titania, Langmuir, 21 (2005) 2552–2559.
[32] M. Laabd, H.A. Ahsaine, A. El Jaouhari, B. Bakiz, M. Bazzaoui, M. Ezahri, A. Albourine, A. Benlhachemi, Congo red removal by PANi/Bi_2WO_6 nanocomposites: kinetic, equilibrium and thermodynamic studies, J. Environ. Chem. Eng., 4 (2016) 3096–3105.
[33] W. Wang, J. Xu, L. Zhang, S. Sun, Bi_2WO_6/PANI: an efficient visible-light-induced photocatalytic composite, Catal. Today, 224 (2014) 147–153.
[34] C. Li, G. Chen, J. Sun, Y. Feng, J. Liu, H. Dong, Ultrathin nanoflakes constructed erythrocyte-like Bi_2WO_6 hierarchical architecture *via* anionic self-regulation strategy for improving photocatalytic activity and gas-sensing property, Appl. Catal., B, 163 (2015) 415–423.
[35] D. Wang, G. Xue, Y. Zhen, F. Fu, D. Li, Monodispersed Ag nanoparticles loaded on the surface of spherical Bi_2WO_6 nanoarchitectures with enhanced photocatalytic activities, J. Mater. Chem., 22 (2012) 4751–4758.
[36] X. Zhao, H. Yang, S. Li, Z. Cui, C. Zhang, Synthesis and theoretical study of large-sized $Bi_4Ti_3O_{12}$ square nanosheets with high photocatalytic activity, Mater. Res. Bull., 107 (2018) 180–188.
[37] L. Zhou, W. Wang, S. Liu, L. Zhang, H. Xu, W. Zhu, A sonochemical route to visible-light-driven high-activity $BiVO_4$ photocatalyst, J. Mol. Catal. A: Chem., 252 (2006) 120–124.
[38] A. Kudo, I. Tsuji, H. Kato, $AgInZn_7S_9$ solid solution photocatalyst for H_2 evolution from aqueous solutions under visible light irradiation, Chem. Commun., 17 (2002) 1958–1959.
[39] Y.-j. Hao, F.-t. Li, F. Chen, M.-j. Chai, R.-h. Liu, X.-j. Wang, In situ one-step combustion synthesis of Bi_2O_3/Bi_2WO_6 heterojunctions with notable visible light photocatalytic activities, Mater. Lett., 124 (2014) 1–3.
[40] L. Li, X. Wang, Y. Lan, W. Gu, S. Zhang, Synthesis, photocatalytic and electrocatalytic activities of wormlike $GdFeO_3$ nanoparticles by a glycol-assisted sol–gel process, Ind. Eng. Chem. Res., 52 (2013) 9130–9136.
[41] I.K. Konstantinou, T.A. Albanis, TiO_2-assisted photocatalytic degradation of azo dyes in aqueous solution: kinetic and mechanistic investigations: a review, Appl. Catal., B, 49 (2004) 1–14.
[42] W.J. Kim, D. Pradhan, B.-K. Min, Y. Sohn, Adsorption/photocatalytic activity and fundamental natures of BiOCl and $BiOCl_xI_{1-x}$ prepared in water and ethylene glycol environments, and Ag and Au-doping effects, Appl. Catal., B, 147 (2014) 711–725.
[43] C. Chang, L. Zhu, S. Wang, X. Chu, L. Yue, Novel mesoporous graphite carbon nitride/BiOI heterojunction for enhancing photocatalytic performance under visible-light irradiation, ACS Appl. Mater. Interfaces, 6 (2014) 5083–5093.
[44] X. Wang, P. Tian, Y. Lin, L. Li, Hierarchical nanostructures assembled from ultrathin Bi_2WO_6 nanoflakes and their visible-light induced photocatalytic property, J. Alloys Compd., 620 (2015) 228–232.
[45] X. Zhao, H. Yang, Z. Cui, X. Wang, Z. Yi, Growth Process and CQDs-modified $Bi_4Ti_3O_{12}$ Square Plates with Enhanced Photocatalytic Performance, Micromachines (Basel), 10 (2019) 66.